Sci. Rep. Kanazawa Univ.
Vol. 38 No.1,2 pp. 59~77
December 1993

Processes of Formation of Bacterial Iron and Carbon Minerals

Kazue TAZAKI

Department of Earth Sciences, Faculty of Science, Kanazawa University, Kakuma, Kanazawa 920-11, Japan

Abstract: Lepidocrocite, hematite, and graphite associated with fossilized bacterial cells have been detected in 2.0 Ga cherts from the Canadian Gunflint Iron Formation by XRD, ESCA, EPMA, and TEM. Filamentous and coccoid morphologies on bacteria occur inside accumulations composed predominates of Si and Fe, and trace amounts of Al, Mg, and C. The ancient microorganisms probably served as nucleation sites for the precipitation of iron, first lepidocrocite, which later was transformed during diagenesis to hematite. As the living cells were transformed, organic carbon first gave way to low crystalline carbon minerals, which later were transformed to well-crystalized graphite.

In recent sediments receiving acid drainage from mine tailing and coal refuse impoundments in a variety of iron oxides precipitate. The major iron oxide is ferrihydrite which later transforms to goethite or hematite. These data from recent sediments are of use in interpreting ancient processes and environments. Fe precipitation in the ancient bacterial cells may have been similar to processes that deposit iron in recent acidic sediments.

1. Introduction

Walter (1976), Awramik and Barghoorn (1977) and Knoll et al. (1978) reported Gunflint-type microbiotas, new microorganisms and stromatolites of the Gunflint Iron Formation. In siliceous and metalliferous sedimentary rocks, bacterial cell walls have been implicated in the formation of new minerals (Houot et al., 1984; Robert and Berthelin, 1986; Southgate, 1986). Electron microscopic studies have shown that bacteria are capable of serving as nucleation sites for authigenic formation of minerals (Beveridge et al., 1983; Ferris et al., 1986, 1987).

In this study, bacterial cells in 2.0 Ga year old cherts were analyzed and compared to mineralized modern bacteria in recent sediments from acid mine drainage environments. The mineralogical composition of Precanbrian cherts and recent sediments were evaluated by X-ray powder fiffraction (XRD), Secondary iron mass spectroscopy (SIMS), electron spectrochemical surface analysis (ESCA), and electron microprobe analysis (EPMA) were used to determine elemental distributions. Bacterially associated mineralization was observed by transmission electron microscopy (TEM) and selected area electron diffraction (SAED).

2. Materials and Methods

Stromatolitic red and gray cherts of the 2.0 Ga Gunflint Iron Formation from the Mink Mountain, Schreiber, Northern Ontario, were studied. These were compared with recent

sediments that were collected from seepage area near inactive mine-tailing ponds at Burchell Lake (west of Thunder Bay), Cranberry Lake (north west of Sudbury) in Canada and in Belmont Country, Ohio, USA (Ferris et al., 1988, 1989).

Rock and sediment samples were ground in water in a mortar; the resulting 2 μm fraction was then decanted, and the supernatant suspension was studied by XRD using a Rigaku goniometer having Cu Kα radiation, operated at 40 kV and 20 mA. TEM observation was carried out on the 2 μm-size-fraction and ultra-thin section, using JEOL -EM 100C and a JEOL-2000EX instruments having accelerating voltages of 100 or 200 kV respectively. Both instruments were operated using a liquid-nitrogen-cooled anticontamination device in place at all times. Upon sampling living specimens were immediately fixed with 1.0 % (v/v) aqueous glutaraldehyde, a biological fixative used in electron microscopy.

Au-coated-polished thin section of a rock sample was in the analysis of individual bacterial cells. Electron microprobe spectra were collected with a JEOL, JXA8600 superprobe. The instrument was operated at 15 kV on the thin section for qualitative and quantitative chemical analyses.

The fine suspensions were recovered with a pipet and dispersed on glass slides. A Cameca IMS-3F spectrometer was used for SIMS; Bar-graphs were obtained from these thin films using a mass filtered 100 μm diameter $^{16}O^-$ ion beam having primary and secondary accelerating voltages of 12.5 and 4.5 KeV, respectively.

Electron spectrochemical analyses (ESCA) were conducted using a SSX-100 X-ray photoelectron spectrometer equipped with a custom-designed vacuum system and sample treatment chember. The samples were mounted on copper grida. A monochromatized Al Kα X-ray excitation beam was used, and all binding energy levels were referenced to 1s C at 285.0 eV.

3. Results

3.1 Ancient bacteria in Precambrian cherts

Stromatolitic red and gray cherts were analyzed by XRD, EPMA, ESCA, and TEM as follows;

3.1.1 XRD

The XRD patterns of gray chert (A) and red chert (B) reproduced in Figure 1 showed the presence of strong quartz peaks, broad lepidocrocite (6.3 Å and 1.9 Å), small sharp hematite (2.7 Å), calcite (3.0 Å), and graphite (2.08 Å) peaks. Other electron microtechniques confirmed the presence of contained organic matter, a trace of altered feldspar, and sulphate.

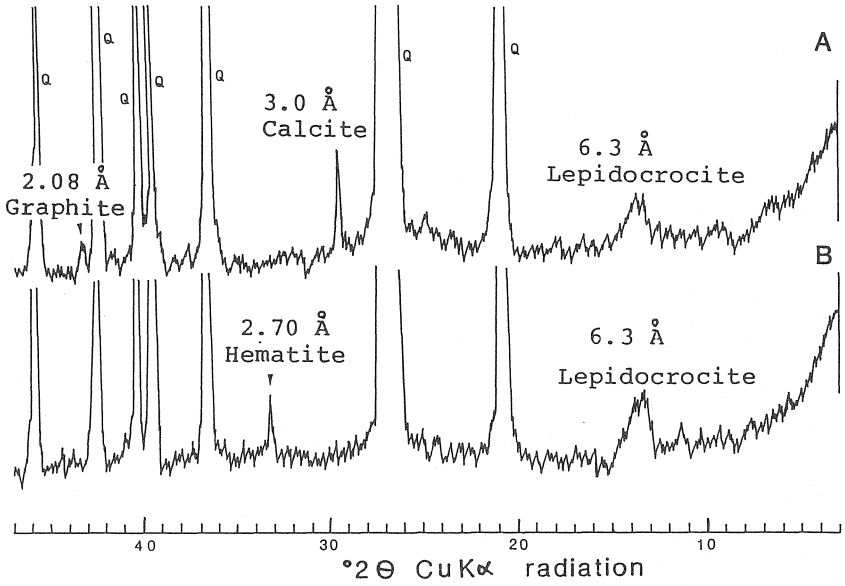

Fig. 1. X-ray powder diffraction patterns of gray chert (A) and red chert (B) from the Gunflint Iron Formation, Canada. Q: quartz.

3.1.2 Optical microscopy

Optical micrographs of a gray chert thin section showed coccoid (Fig. 2A) and filamentous bacterial communities in which individual cells appear to be well preserved by silicification. Coccoids having high optical density and opaque cell walls suggest the presence of iron oxide coating (Fig. 2B). Cell division and binary fission patterns are observed. The matrices surrunding iron-loaded cell walls consisted of granular crystallites (Fig. 2B).

3.1.3 Electron microprobe analysis

The distribution pattern of metal ions in the thin section indicated difference in chemistry between grain and matrix components (Fig. 3). The Fe Kα content map (B) vealed the presence of iron in both coccoid and filamentous (arrows in Fig. 3) bacterial communities, and revealed remains of bacteria inside iron accumulations. Altered feldspar in the centre of the map has a high iron profile. The Si Kα content map (C) clearly shows that the matrix is rich in Si, consistent with quartz. Chemical analyses of spherical bacteria in the gray chert, from electron microprobe spectra, show that an individual bacterial cell is composed of mainly Si, Fe, and O (Fig. 4).

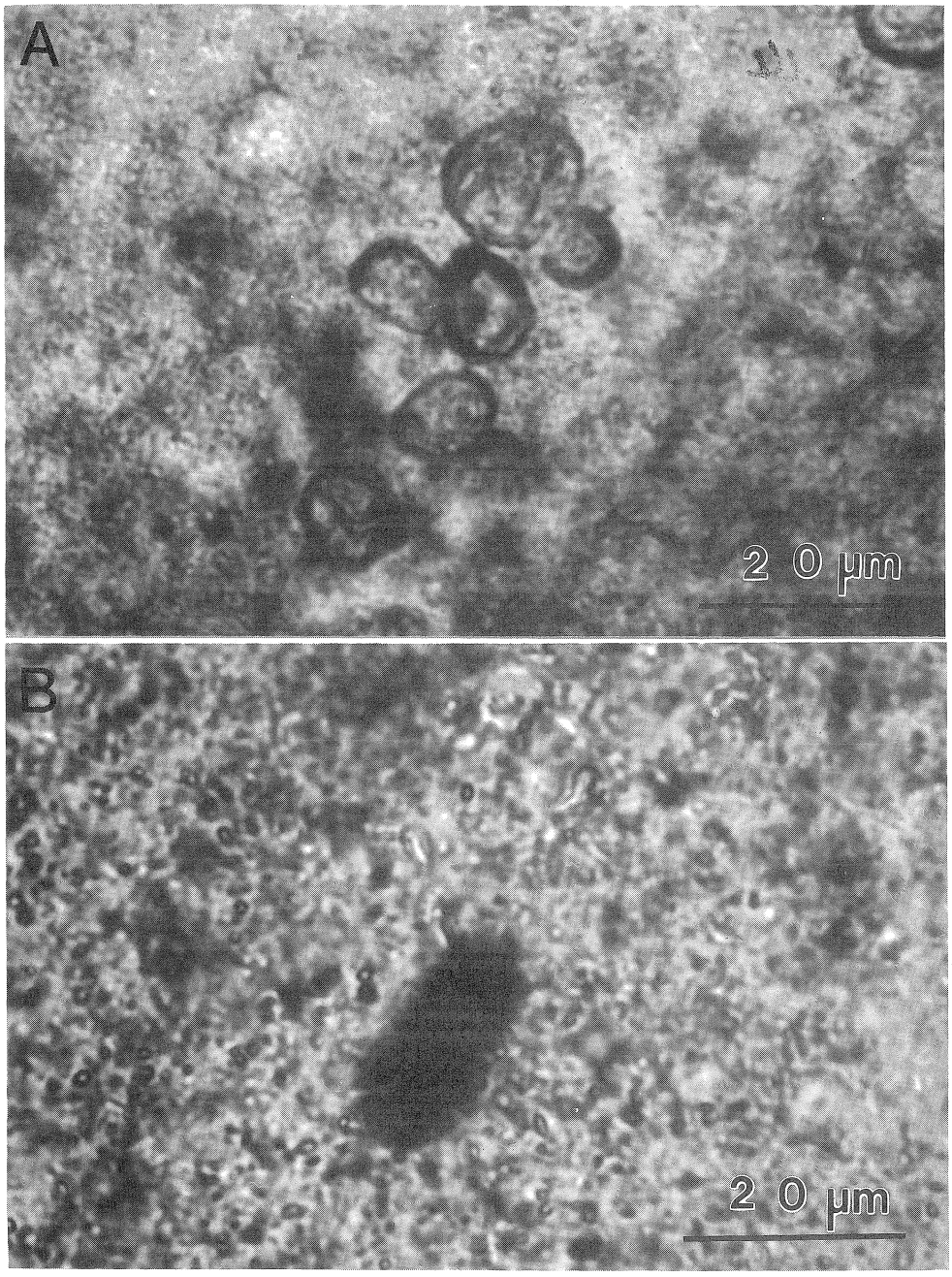

Fig. 2. Optical micrographs of gray chert thin section showing (A) silicified coccoid cyanobacterial communities, and (B) opaque, iron-loaded bacterial cell in the granular crystallites. (Light color is quartz, and dark color is iron oxide).

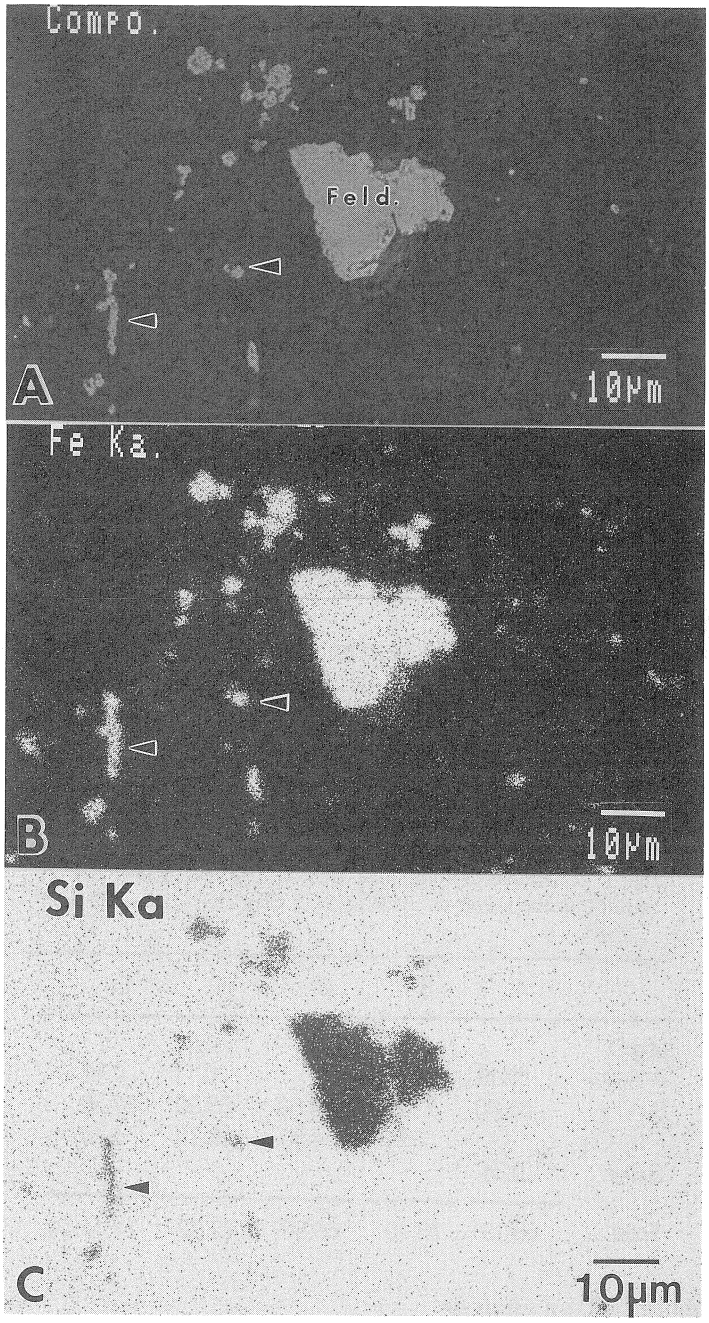

Fig. 3. Electron microprobe analyses of polished-thin section of red chert showing (A) compositional image, (B) high concentration of Fe Kα in the filamentous and coccoid cyanobacterium (arrows), and (C) wide distribution of Si Kα

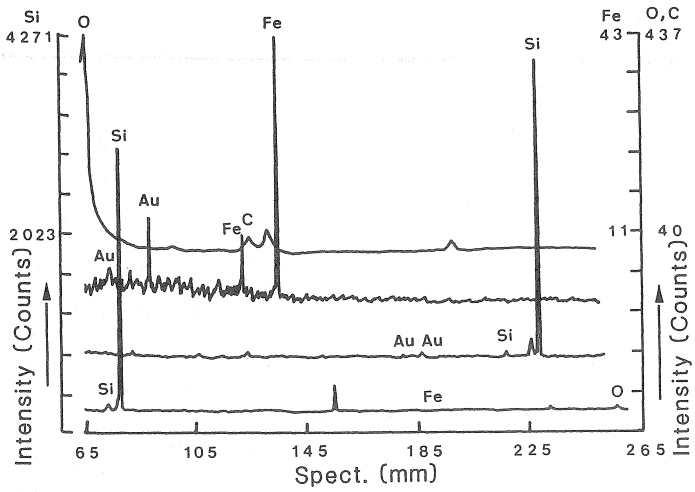

Fig. 4. Electron microprobe spectra from one individual coccoid cell in the polished-thin section of gray chert. Si, O and Fe concentration are high, while C occurs in trace amounts. Sample was coated by Au.

The quantitative analyses from electron microprobe spectra confirmed silicification in all and condensation of Fe_2O_3 in most coccoid cells (Table 1). Trace amount of MgO, Al_2O_3, and SO_3 are also recognized. The chemistry of coccoid cells in gray chert (A, B and C in Table 1) and red chert (D and E) shows variable quantity of Fe in cells. The low total percentage suggests that carbon and fluid H_2O remain in these cells.

Table 1. Chemical analyses of coccoidal bacteria from electron microprobe spectra. A, B and C ; gray chert, D and E ; red chert.

	A	B	C	D	E
MgO	-	-	-	0.21	-
Al_2O_3	0.19	-	-	0.11	0.12
SiO_2	65.60	71.60	64.60	65.30	67.32
Fe_2O_3	-	3.50	4.90	6.70	3.67
SO_3	0.34	-	-	-	-
Total	66.13	75.10	69.50	72.32	71.11 %

3.1.4 X-ray photoelectron analysis

The ESCA spectrum of the whole powder sample showed high concentration of Si and O, with traces of Fe, Na, Ca, Mg, C, and Al, as would be expected for a quartz matrix and calcite in the gray chert (Fig. 5 and Table 2). The XRD and ESCA results are based on bulk samples, which are averaged measurements. Even so, about 19 % of 1s C is present in the chert.

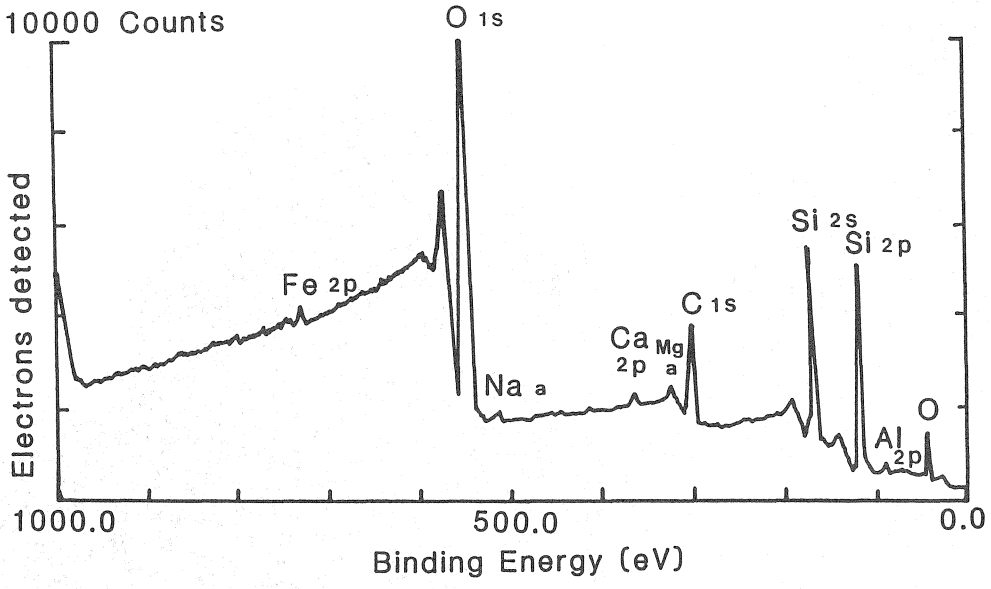

Fig. 5. X-ray photoelectron spectro-analysis of powder sample of gray chert showing high concentration of C 1s, Si 2s and 2p, and O 1s.

Table 2. Chemical analyses of powder sample of gray chert from X-ray photoelectron spectra.

Elem.		Atom %	
Fe	2p	0.13	0.10
O	1s	52.04	51.89
Ca	2p	0.42	0.51
C	1s	18.96	19.02
Si	2p	28.06	27.55
Mg	a	0.39	0.93
	Total	100.00	100.00

3.1.5 TEM observations

Iron-mineralization

TEM micromorphology of individual bacterial cells revealed the mineralization processes which contributed to the preservation of the cells in cherts (Fig. 6-9). Coccoid microfossils in the chert showed a condensation of ferric granular particles on the cell walls (Figs. 6 and 7). A large aggregate of coccoid cells becoming mineralized with iron shows the process, from 1 to 3 (Fig. 6). The incipient crystallization of the walls showed weak electron diffraction rings at 4.2 Å, suggesting the presence of goethite. Formation of

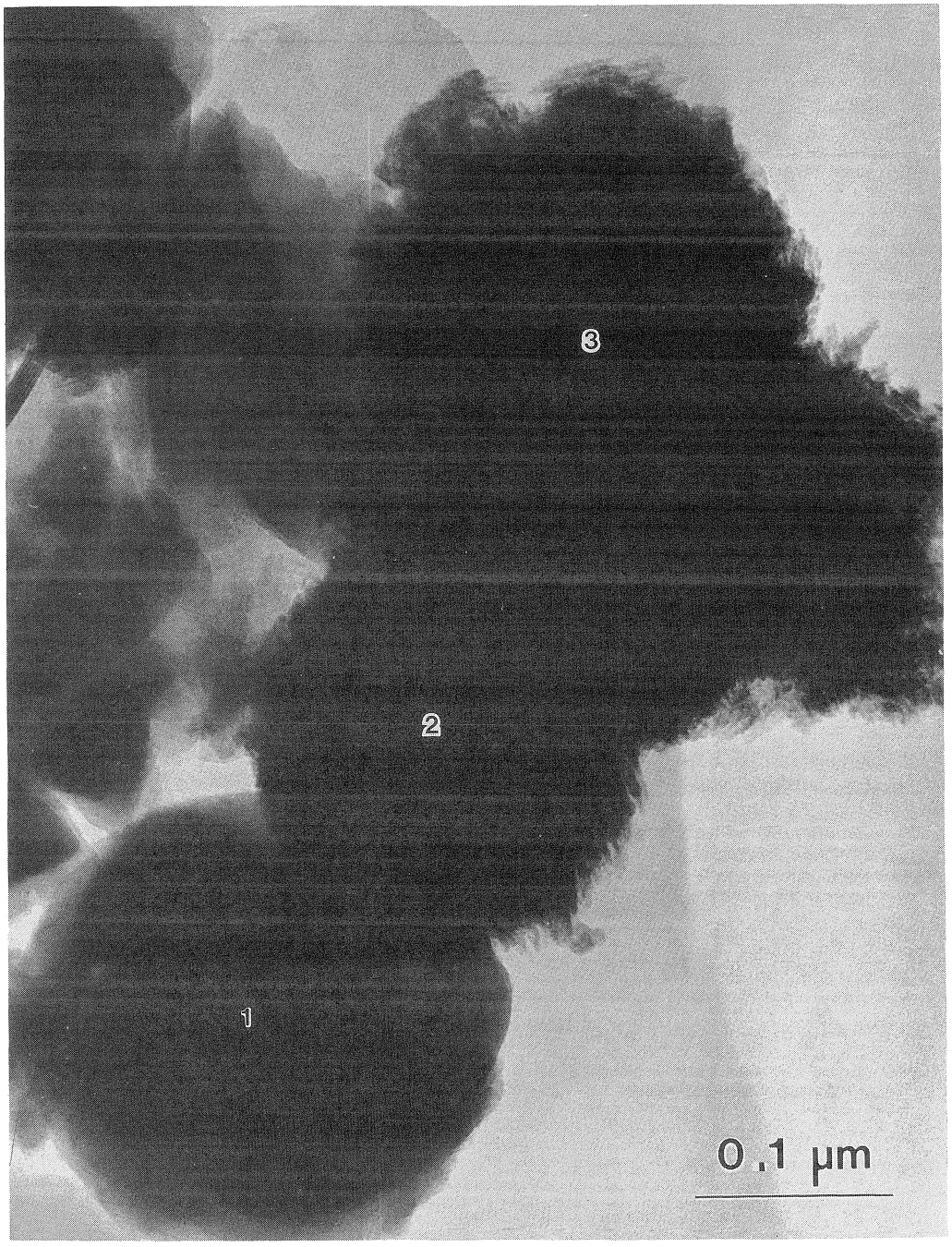

Fig. 6. Transmission electron micrograph of iron-loaded bacterial cells. 1; no iron-present on cell, 2; iron-loaded cell, 3; subsequent mineralization of amorphous iron to goethite or hematite.

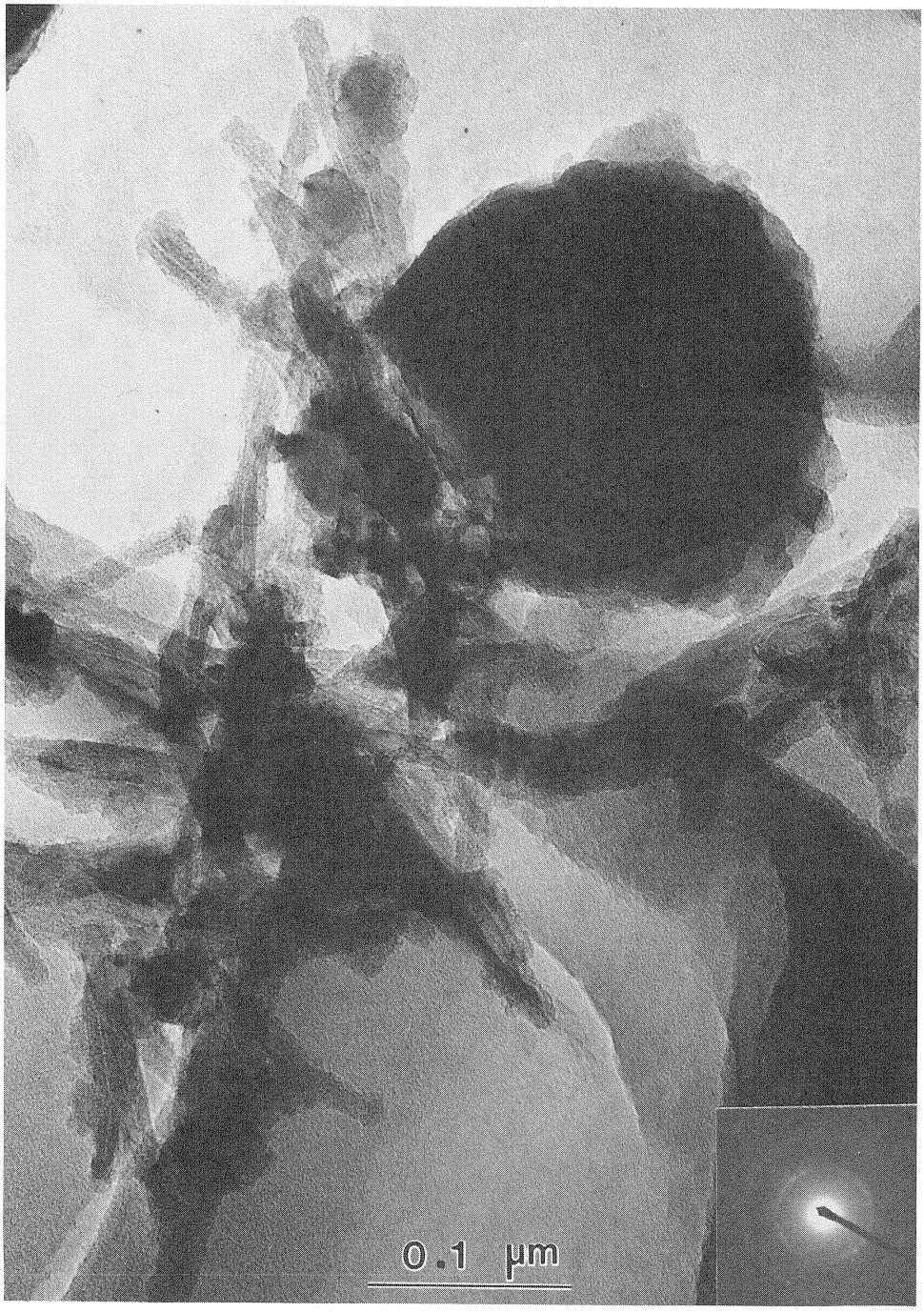

Fig. 7. Transmission electron micrograph of hematite blades associated with coccoid bacterial cell. The electron diffraction (inset) shows spots at 2.56, 2.47 and 1.70 Å.

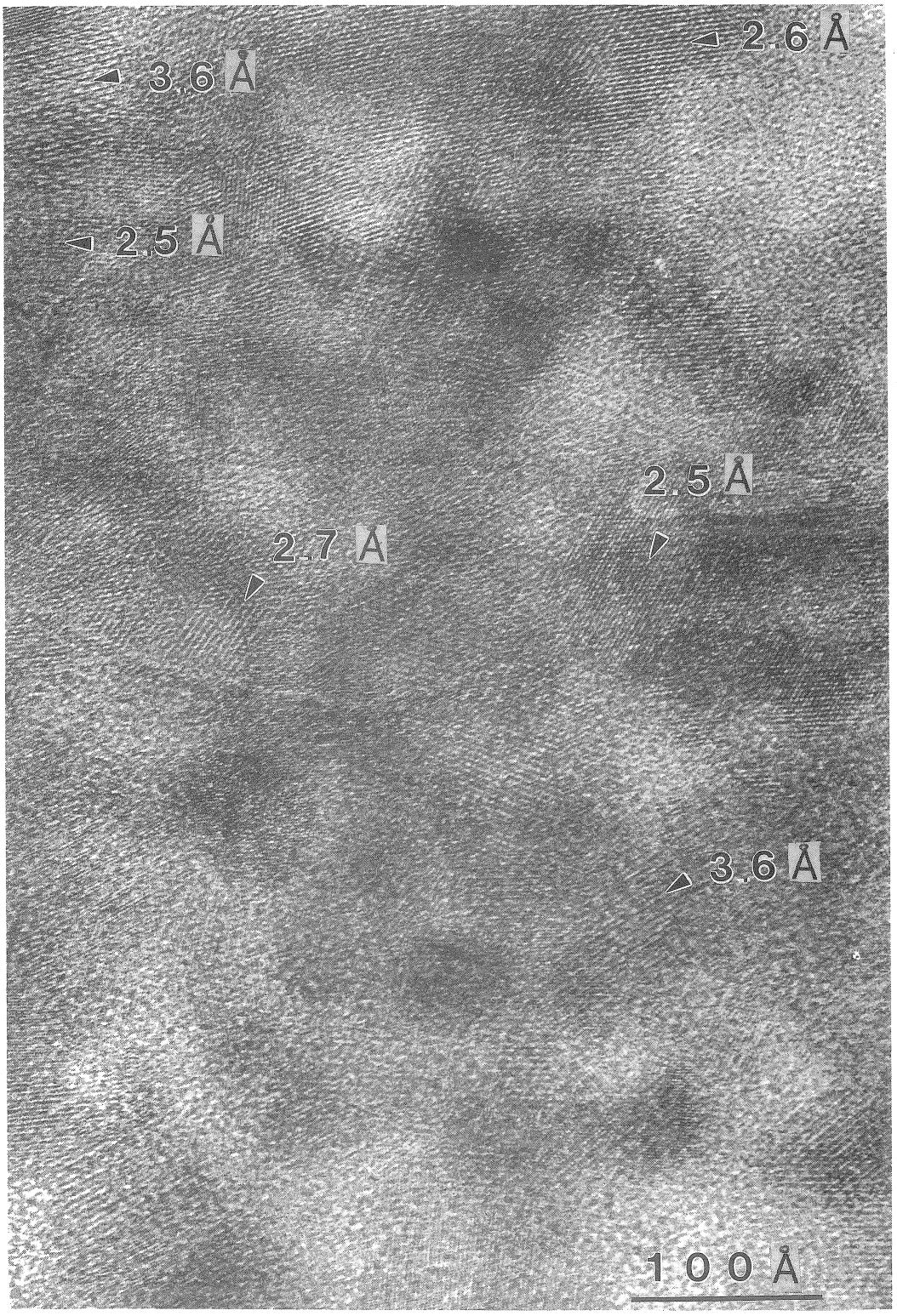

Fig. 8. High-resolution of transmission electron micrograph of hematite associated with bacterial cell, showing mosaic lattice images of hematite crystallite d-spacings.

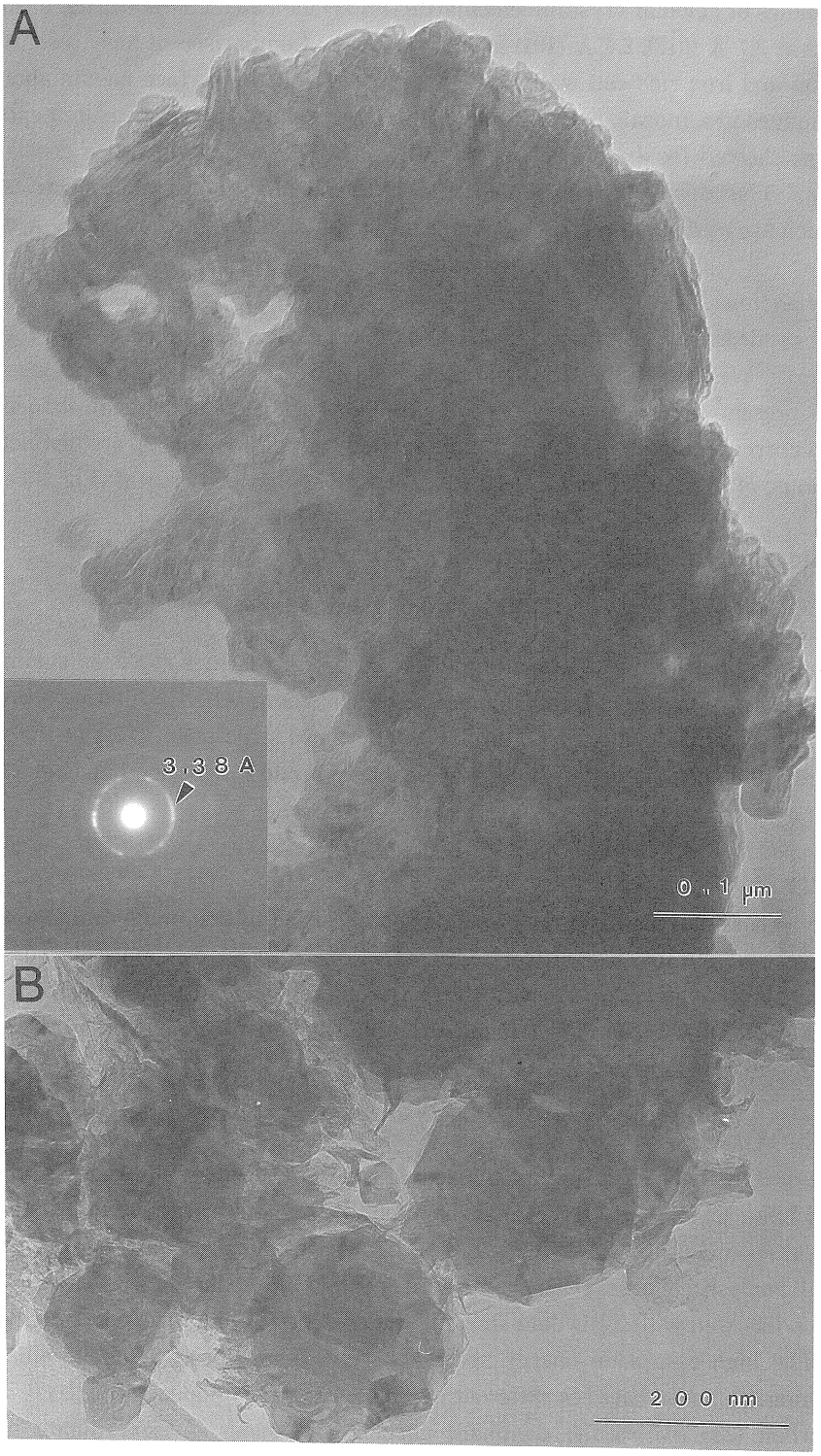

Fig. 9. Transmission electron micrograph of graphitization associated with elongated bacterial cell. The electron diffraction shows characteristic graphite d-spacing at 3.38 Å (002) (A, inset). B; Crystalline graphite associated with bacterial cell shows spiral, hexagonal or curled-sheets structures.

large bundles of acicular crystalline hematite (Fig. 7) indicated characteristic d-spacings of hematite at 3.7 Å (012), 2.7 Å (104) and 2.5 Å (110). Comparison of high-resolution TEM of no iron and iron rich cell walls, clearly revealed that the surface has an abundance of lattice images in a mosaic pattern (Fig. 8). High-resolution TEM measurements of the d-spacings, showed localized 2.5, 2.6, 2.7 and 3.6 Å d-spacings which are consistent with hematite. The mosaic structure also showed the localization of high electrical density sites which are as distinct nuclei for the formation of lepidocrocite having a 6 Å d-spacing.

Graphitization

The condensation and mineralization of the once organic materials were found in the gray chert. Well-crystallized graphite showing 3.38, 2.04 and 1.23 Å spacings (Fig. 9A inset) is present in well preserved cells. Single spiral and hexagonal shaped crystals having a corresponding strong electron diffraction spot at 3.4 Å (002), are distinctly higher crystallinity of graphite (Fig. 9B) than that of cylinder-shaped crystal (Fig. 9A).

3.2 Bacteria in present sediments

3.2.1 XRD

Mineral composition of acid mine drainage sediments at six places summarized in Table 5. The XRD results from Ohio had a mineral composition exhibiting a broad weak reflection suggesting small crystal size and amorphous structure. Most of the sediments contained an abundance of ferrihydrite which gave broad diffraction bands at 2.5, 2.2 and 1.5 Å.

3.2.2 SIM

The SIMS analyses gave the elemental composition of acid mine drainage sediments at six places (Table 3). A significant enrichment of C, Mg, Al, Si, Ca and Fe were revealed in the most of sediments. Fe was the major metallic element detected by SIMS, as revealed by XRD, whereas Si was found as a major nonmetallic element, as expected from the increased abundance of quartz in the sediments.

3.2.3 ESCA

The surface bulk chemistry of the sediments from Cranberry Lake (A), Ohio (B) and Burchell Lake (C) in Fig. 10 shows that the main ESCA spectra of the sediments are oxygen (1s) and carbon (1s) associated with Fe, N, Ca, Cl, S, and Si. The quantitative surface chemical analyses (Table 4) showed on Fe content of about 7 % in these sediments, corresponding well with XRD data showing the presence of metastable iron oxide mineraloids. The high-resolution energy spectra of C (1s) for these sediment, illustrate the partitioning of carbon between different available carbon compounds (Fig. 11). Note that hydrocarbon (285 eV) is the dominant carbon compound. A subordinate amount of

Table 3. Secondary iron mass spectroscopical analyses of bulk powder samples from acid mine drainage sediments.

	H	Li	Be	B	C	N	O	F	Na	Mg	Al	Si	P	S	Cl	K
ZENMAC	12789	22	42	174	59826	747	13725	23	8882	273310	301360	513380	432	172	60	2310
BURCHEL 2	8725	94	26	528	3188	1258	27115	96	41760	34732	121760	625540	801	1715	0	5146
BURCHEL 3	7859	158	50	214	1732	986	15083	17	28782	16816	63548	321290	180	596	41	4142
OHIO "A"	881	108	34	44	316	268	5515	7	5946	11801	91406	99839	82	58	5	4481
OHIO "B"	7872	12	198	414	276	237	18613	98	23765	12079	919160	171620	817	45	0	143
CRANBERRY LAKE	21493	56	18	146	7931	2382	35120	73	143100	92379	56541	705970	148	1515	64	4550
																CPS

	Ca	Sc	Ti	V	Cr	Mn	Fe	Ni	Co	Cu	Zn	Ga	As	Kr	Rb	Sr	Y	Zr	Nb	Mo
ZENMAC	122700	53	4833	180	350	851	95301	284	11	135	58	13	0	0	0	21	37	15	0	0
BURCHEL 2	41252	55	36456	1082	436	549	813430	2317	11	24	24	7	17	5	7	53	19	105	13	0
BURCHEL 3	16093	19	8130	230	103	162	375710	1007	0	15	3	0	0	0	3	36	0	30	5	0
OHIO "A"	22592	9	1755	44	26	482	275850	819	0	5	7	5	0	7	7	528	9	13	7	0
OHIO "B"	22779	11	430	71	48	233	1223400	3512	0	39	16	11	19	0	0	26	398	9	0	13
CRANBERRY LAKE	141680	11	1619	90	36	168	497090	1469	0	137	5	0	0	0	0	48	5	28	0	7
																			CPS	

	Ba	La	Ce	Pr	Nd	Sm	Eu	Gd	Dy	Er	Th	U
ZENMAC	169	25	36	7	15	0	0	0	0	0	0	0
BURCHEL 2	115	32	57	5	0	0	0	0	0	0	3	21
BURCHEL 3	9	5	3	0	5	0	0	0	0	0	0	3
OHIO "A"	21	0	3	3	0	0	0	0	0	0	0	0
OHIO "B"	232	32	151	46	88	7	5	5	7	7	0	0
CRANBERRY LAKE	26	3	5	0	0	0	0	0	0	0	0	3
												CPS

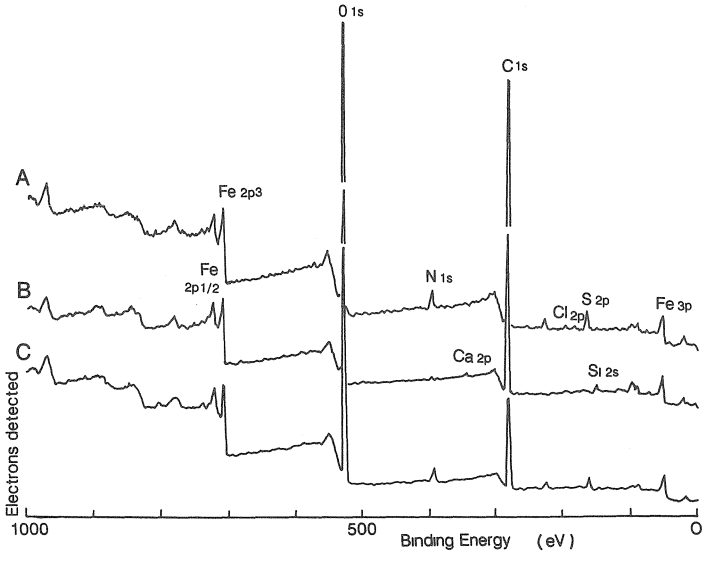

Fig. 10. X-ray photoelectron spectra of bulk sediment samples from Cranberry Lake (A), Ohio (B), and Burchell Lake (C).

Table 4. Surface chemical composition of sediments from Burchell Lake, Ohio, and Cranberry Lake, as determined by X-ray photoelectron spectra.

		BURCHELL	OHIO 'A'	CRANBERRY LAKE
O	1s	41.41	32.95	30.94
N	1s	3.45	0.55	2.02
Ca	2p	-	0.49	-
C	1s	46.59	54.22	57.18
Cl	2p	-	0.26	0.39
S	2p	2.08	0.66	2.22
Si	2p	-	3.47	0.56
Fe	3p	6.47	7.40	6.69
	Total	100.00	100.00	100.00 %

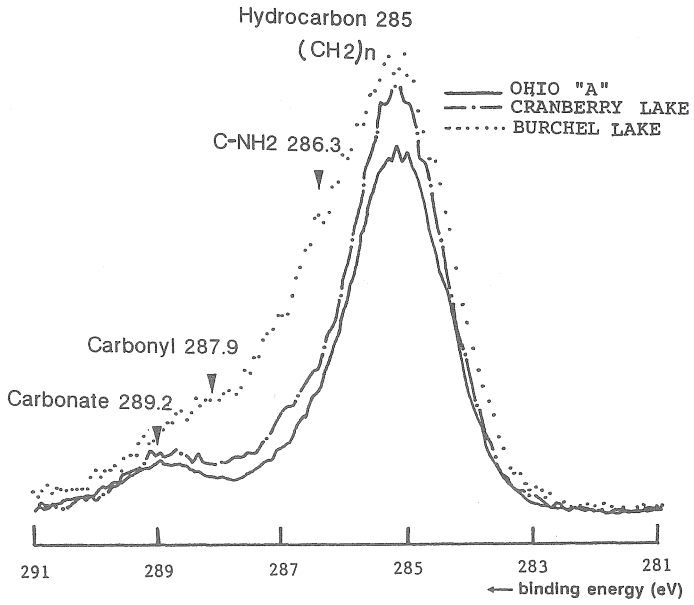

Fig. 11. C 1s of X-ray photoelectron spectra of sediment samples from Ohio, Cranberry Lake, and Burchell Lake.

carbonate (289.2 eV) is also present. The high-resolution energy spectrum of iron (Fe-2p) indicates the presence of an organic component at 712.4 eV, $Fe(C_5H_5)(CO)_3$. Both carbon (1s) and iron (2p) show chemical bondings of organic and inorganic materials, suggest that iron mineralization is associated with the microorganisms.

3.2.4 TEM observations

The whole mounts of acid mine drainage sediments are rich in ferrihydrite, showing two types of morphology; one has radial growth fibrous materials giving the clear electron diffraction spots at 4.9 Å (111) and 3.0 Å (220) of magnetite, Fe_3O_4 (Fig. 12A inset); the second is developed in association with the elongated bacteria (Fig. 12B). Fine granular iron oxide grains are partly attached to the surface of the elongated bacteria giving the broad ring at 2.5 Å of ferrihydrite $5Fe_2O_3 \cdot 9H_2O$.

Ultra-micro-thin-section of the present mud sample from Cranberry Lake revealed remnants of microorganisms having iron oxides heavily precipitated on cell walls (Fig. 13 and Table 5). The microcrystalline aggregate surrounding the wall is goethite. Abundant intracellular and cell wall microcrystalline lepidocrocite (γ-FeOOH) has been identified in the photosynthetic protist Euglena sp. in the mine tailing waters of the Elliot Lake district, where pH < 2 and aqueous Fe averages 560 ppm (Fig. 14). Selected area electron diffraction patterns of the mineral phase yielded spacings at 6.26 (020), 2.79 (011), 2.09 (131, 060), and 1.496 Å (022), signifying lepidocrocite. EDX analysis indicated a strong signal for Fe.

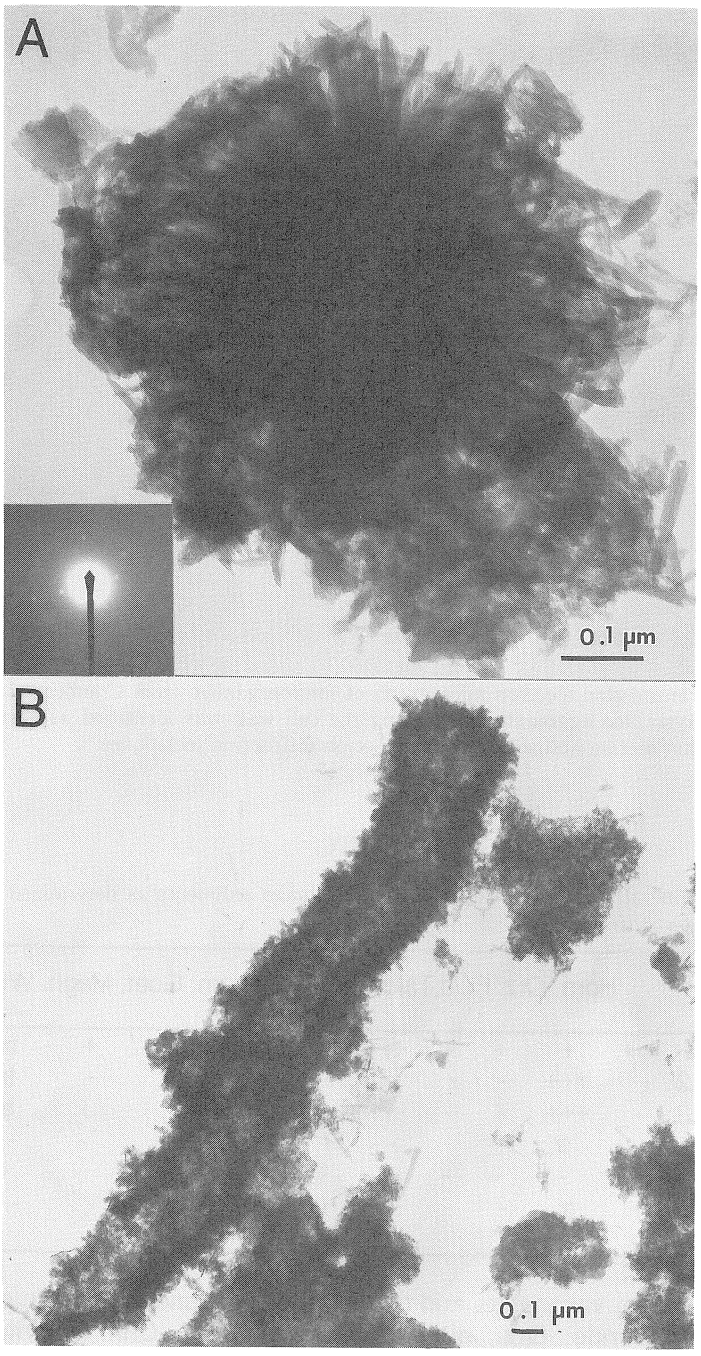

Fig. 12. Fibrous ferrihydrite and the corresponding electron diffraction pattern in a whole mount of sediment from Burchell Lake (A). The electron diffraction pattern shows strong spots of magnetite at 4.9 Å (111) and 3.0 Å (220). B; The granular ferrihydrite of bacterially associated Fe mineralization in the Ohio sediment samples.

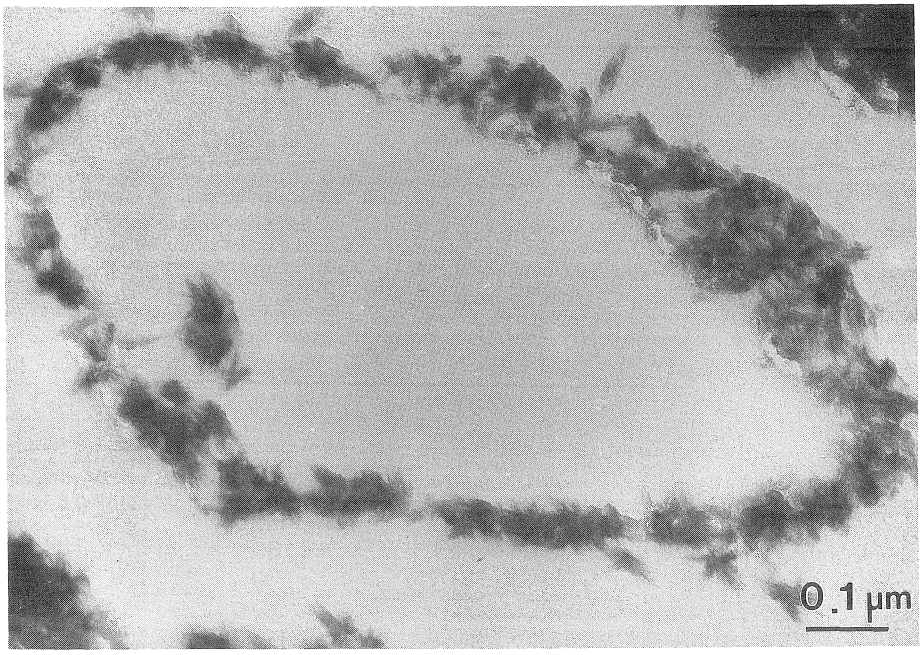

Fig. 13. Transmission electron micrograph of microorganism from Cranberry Lake. The microcrystalline aggregate surrounding the cell wall was identified as goethite using ultra-thin section and selected area electron diffraction techniques.

Table 5. Mineral composition of acid mine drainage sediments as determined by X-ray powder diffraction.

	Horn.	Qtz.	Feld.	Talc	Chl.	Gyp.	Magn.	Goet.	Magh.	Wus.	Hem.
							Ferr.				
ZENMAC	+++	+	+	+	+++	tr.	tr.	+	+	tr.	+
BURCHEL2	-	+++	-	-	tr.	-	++	tr.	-	tr.	tr.
BURCHEL3	-	+++	-	-	tr.	-	++	tr.	-	tr.	tr.
OHIO 'A'	-	tr.	-	-	-	+	+	+	-	-	+
OHIO 'B'	-	-	-	-	-	-	+	+	-	-	tr.
CRANBERRY LAKE*	-	tr.	-	-	-	+	+++	tr.	-	-	tr.

* : Akaganeite, vivianatite, and cordierite were found in this sample.
Horn.: hornblende, Qtz.: quartz, Feld.: feldspar, Chl.: chlorite, Gyp.: gypsum, Magn.: magnetite, Ferr.: ferrihydrite, Goet.: goethite, Magh.: maghemite, Wus.: wustite, Hem.: hematite.

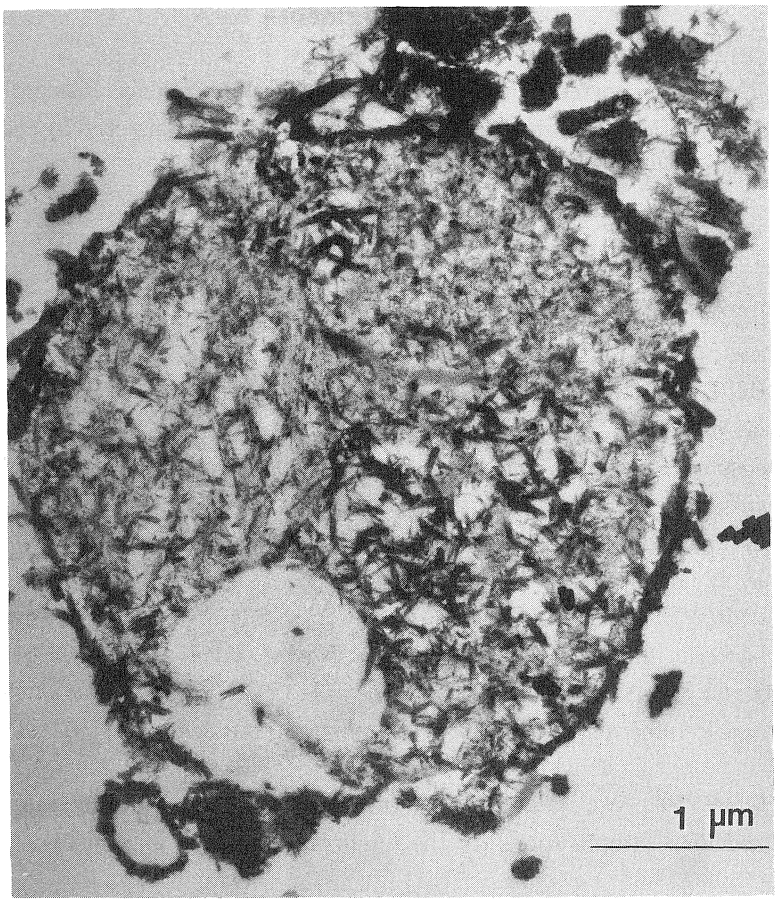

Fig. 14. Euglena sp. (unicellular protist) with intracellular and cell membrane "wall" lepidocrocite, from Elliot Lake, Canada.

4. Conclusions

Ferrihydrite, goethite, lepidocrocite, hematite, and graphite were identified by electron microtechniques in 2.0 Ga cherts and in recent acidic sediments. Electron microscopy and electron microprobe analyses showed that individual bacterial cells promoted the development of iron oxide mineralization and become graphitized. Individual bacterial cells were seen encrusted, showing a sucessive formation process from ferrihydrite and goethite to lepidocrocite and hematite. These bacteria not only served as nucreation sites for the initial deposition of Fe, but also their organic remains were clearly trapped and incorporated into graphite. Both iron and graphite mineralization associated with the bacteria in the cherts suggest that ancient microorganisms resembled present day bacteria in their mineralization and condensation of metal ions as reported by Oehler (1976), Beveridge and Fyfe (1984), Nealson (1983), Ferris et al. (1987, 1988, 1989), Mann et al. (1987), Tazaki et al. (1990, 1992 a, b,) and Tazaki (1993).

Acknowledgments

This work was supported by grants from the National Science Research Fund and International Scientific Research Program; Joint Research, administered by the Monbusho (Japanese Ministry of Education, Science and Culture).

References

AWRAMIK, S.M. and BARGHOORN, E.S., (1977). The Gunflint microbiota. *Precambrian Rese.* , 5, 121-142.

BEVERIDGE, T.J., MELOCHE, J.D., FYFE, W.S. and MURRAY, R.G.E., (1983). Diagenesis of metals chemically complexed to bacteria — Laboratory formation of metal phosphates, sulfides, and organic condensates in artificial sediments. *Applied and Environmental Microbiology*, 45, 1094-1108.

BEVERIDGE, T.J. and FYFE, W.S., (1984). Metal fixation by bacterial cells. *Can. J. Earth Sci.*, 22, 1893-1898.

FERRIS, F.G., BEVERIDGE, T.J. and FYFE, W.S., (1986). Iron-silica crystallite nucleation by bacteria in a geothermal sediment. *Nature* (London), 320, 609-611.

FERRIS, F.G., FYFE, W.S. and BEVERIDGE, T.J., (1987). Bacteria as nucleation sites for authigenic minerals in a metal-contaminated lake sediment. *Chem. Geol.*, 63, 225-232.

FERRIS, F.G., FYFE, W.S. and BEVERIDGE, T.J., (1988). Metallic ion binding by *Bacillus subtilis* — Implications for the fossilization of microorganisms. *Geology*, 16, 149-152.

FERRIS, F.G., TAZAKI, K. and FYFE, W.S., (1989). Iron oxides in acid mine drainage environments and their association with bacteria. *Chem. Geol.*, 74, 321-330.

HOUOT, S., CESTRE, T. and BERTHELIN, J., (1984). Origine du fe conditions de formation du colmatage ferrique — Etudes de differentes situations en France. *In Proc. 11th Congr. Int. Irrigations and Drainage, Fort Collins, Co*, 151-180.

KNOLL, A.H., BARGHOORN, E.S. and AWRAMIK, S.M., (1978). New microorganisms from the Aphebian Gunflint Iron Formation, Ontario. *J. Paleont.*, 52, 976-992.

MANN, H., TAZAKI, K., FYFE, W.S., BEVERIDGE, T.J. and HUMPHREY, R. , (1987). Cellular lepidocrocite precipitation and heavy-metal sorption in *Euglena sp.* (unicellular alga) — Implications for biomineralization. *Chem. Geol.*, 63, 39-43.

NEALSON, K.H., (1983). The microbial iron cycle. *In* KRUMBEIN, W.E., ed. *Microbial Geochemistry:* Blackwell Scientific, Oxford, 159 -190.

OEHLER, J.H., (1976). Experimental studies in Precambrian paleontology — structural and chemical changes in blue-green algae during simulated fossilization in synthetic chert. *Geol. Soc. Amer. Bulletin*, 87, 117-129.

ROBERT, M. and BERTHELIN, J., (1986). Role of biological factors in soil mineral

weathering. *In* HUANG, P.M. and SCHNITZER , M., eds., *Interaction of Soil Minerals with Natural Organics and Microbes: Soil Sci. Soci. of Amer. Inc.*, Madison, Wisconsin, USA, 453-495.

SOUTHGATE, P.N., (1986). Depositional environment and mechanism of preservation of microfossils, upper Proterozoic Bitter Springs Formation, Australia. *Geology*, 14, 683-686.

TAZAKI, K., FERRIS, F.G., WIESE, R.G. and FYFE, W.S., (1990). Bacterial lepidocrocite and hematite in chert. *Proceedings of 9th Inter. Clay Conf.*, Strasbourg, France, 1, 35-44.

TAZAKI, K. and FYFE, W.S., (1992a). Microbial green marine clay. *Chem. Geol.*, 102, 105-118.

TAZAKI, K., MORI, T. and NONAKA, H., (1992b). Microbial jarosite and gypsum from corrosion of Portland cement concrete. *Canadian Mineralogist*, 30, 431-444.

TAZAKI, K., (1993). The sulfides and sulfate complexes with bacteria in the Earth environment. *Earth Science (Chikyu Kagaku)* , 47, 251-270 (in Japanese with English abstract).

WALTER, M.R., (1976). Stromatolites. Elsevier Scientific Publishing Comp., Amsterdam-Oxford-New York.